EPJ Web of Conferences **94**, 04010 (2015)
DOI: 10.1051/epjconf/20159404010

The terminal effects of chisel-shape projectile penetrating into metallic target plates

Xu Tao[1,2], Xiaohu Yao[1], and Wei Ma[2,a]

[1] School of Civil Engineering and Transportation, South China University and Technology, Guangzhou 510640, China
[2]Institute of Mechanics, Chinese Academy of Sciences, Beijing 100190, China

Abstract. This work performs the analysis and simulation investigations of penetration behaviors of chisel-shape projectile. In analysis, the projectile is assumed to be a rigid body and the target plate is elastic-plastic material. By introducing the velocity potential function, the velocity field in target is first obtained. Then, the momentum equation is solved for determining the pressure and stress fields in the elastic and plastic regions in target. The variation of the resultant force subjected by the projectiles with the penetration depth is studied. The approximate expressions of penetration depth and the residual velocity with the initial impacting velocity are obtained for the exploration of the penetration mechanisms of the chisel-shape projectile. In numerical simulation, the main attention focuses on the dissipation mechanisms of the kinetic energy of the chisel-shape projectile in penetration process.

1. Introduction

The geometric effect of projectile on the failure behaviors of the target material has drawn great attention in academia and engineering since it determines, to a great extent, the terminal effects of penetration. The previous studies mainly deal with the penetration behaviors of projectiles with conical, hemispherical, flat and ogival configurations. Bishop et al. [1] proposed the cavity expansion model and used the model to estimate the forces of conical-shape projectile of punching slowly into metal targets. Goodier [2] used the cavity-expansion theory to predict the penetration depth of rigid spheres launched into metal targets and to study the penetration behaviors of non-compressible strain hardening material. Forrestal et al. [3,4] studied by penetration experiments the influences of target material constitutive behaviors on the penetration mechanism of different projectile configurations. Chen et al. [5] studied the terminal effects of flat projectile penetrating into metallic target and demonstrated the shear failure mechanism of target board material in penetration. Alekseevskii [6] and Tate [7,8] developed an inviscid flow model for projectile and target material which depicts the velocity field of target material in high-speed collision between projectile and target plate. Ravid et al. [9,10] used this model to research the failure mechanism of metallic plates and the evolution of velocity field at high impacting velocity. Yarin and Rubin [11, 12] established the penetration model by introducing a velocity potential function and analyzed two-dimensional transient stress fields in target for several projectile nose shapes and dynamic phenomena in highly penetration process. Recently, Jordan and Naito [13] carried out an experimental investigation of the effects of nose shape on fragments penetrating E-Glass/Phenolic glass fiber reinforced plastic targets. Initial velocity, residual velocity, and ballistic limit velocities were determined for each nose shape and target thickness. However, it is still a lack of the documents on the studies of the penetration mechanism of chisel-shape projectile into metal target plate.

In this work, the penetration mechanisms of chisel-shape projectile into metal target plate are studied. The penetration model of Yarin et al. [9] is developed to obtain an approximate solution of normal penetration problem of a chisel-shape projectile into elastic-plastic target plates. Through the analysis of stress state in the elastic and plastic regions of target material, the equation of motion of the projectile in the axial direction is solved. The approximate analysis reveals the variations the resultant pressure, penetration depth, kinetic energy dissipation with the initial impact velocity and time. The penetration behaviors of chisel-shape projectile to a finite target plate are investigated.

2. Model and analysis

Consider the problem of normal penetration of a rigid chisel-shape projectile into an elastoplastic target plate. Presently, we assume that the material in plastic deformation region of target is an incompressible fluid and rate-insensitive. The velocity and stress fields in plane strain state are assumed for simplicity. Figure 1 shows the analytic model and the coordinate system $(o; x, y, z)$ with the unit vectors $(\boldsymbol{i}, \boldsymbol{j}, \boldsymbol{k})$ which has a fixed origin o at the front surface of the target. The tip of the projectile is located by $z = w(t)$. The initial impacting velocity is U_0. Furthermore, the projectile body is assumed to have a rectangle cross-section such that to obtain the approximate solution of problem is possible.

[a] Corresponding author: watwm@imech.ac.cn

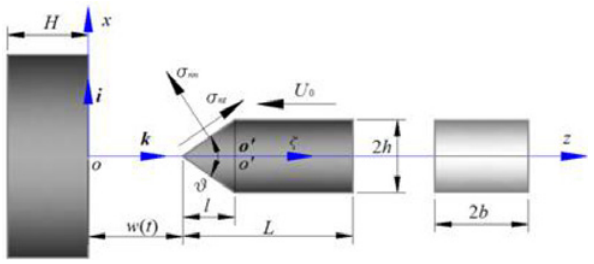

Figure 1. The model for the analysis of the chisel-shape projectile penetration behaviors.

In the following analysis of the penetration behaviors of chisel-shape projectile into metallic target, we adopt the analytic method of Yarin et al. [9] to the mathematic derivation and calculus. The approximate velocity field is first determined by introducing a velocity potential $\phi(x, z, t)$ and then the stress field in target is calculated. Thus, we have the velocity vector expression as follows

$$\mathbf{v} = \nabla\phi, \qquad \nabla^2\phi = 0 \tag{1}$$

the momentum balance equations:

$$\nabla\left[\rho\left\{\frac{\partial\phi}{\partial t} + \frac{1}{2}\nabla\phi\cdot\nabla\phi\right\} + p\right] = \mathrm{div}\mathbf{s} \tag{2}$$

the conservation condition of mass:

$$\mathrm{div}\ \boldsymbol{v} = 0. \tag{3}$$

The Cauchy stress tensor σ has been separated into a hydrostatic pressure p and the stress deviatoric part $\mathbf{s}$:

$$\boldsymbol{\sigma} = -p\mathbf{I} + \mathbf{s}, \qquad \mathbf{s}\cdot\mathbf{I} = 0 \tag{4}$$

where $\mathbf{I}$ denotes the unit tensor and the deviatoric stress $\mathbf{s}$ is determined as

$$\mathbf{s} = 2\mu\boldsymbol{\varepsilon}^e + \left(\frac{2}{3}\right)^{1/2}\frac{\tau_S}{(\dot{\boldsymbol{\varepsilon}}^p\cdot\dot{\boldsymbol{\varepsilon}}^p)^{1/2}}\dot{\boldsymbol{\varepsilon}}^p \tag{5}$$

where ε^e is the elastic strain and $\dot{\varepsilon}^p$ is the rate of plastic deformation tensor. $\boldsymbol{\tau_s}$ is the shear yield stress. The chisel-shape projectile is assumed to be a two-dimensional body for the simplicity in below analysis and the chisel-shape nose lateral profile is defined by

$$x = \begin{cases} \tan\theta\xi + h & (-l \le \xi \le 0, 0 \le y \le b) \\ h & (0 \le \xi \le L - l, 0 \le y \le b) \end{cases} \tag{6a}$$

$$\xi = z - w(t) - \frac{h}{\tan\theta} \tag{6b}$$

ξ is an axial coordinate measured from the point o' in projectile (Fig. 1) and 2θ denotes the chisel angle.

The velocity field is found as

$$v_x = -\dot{w}(t)\frac{h}{\tan\theta}\frac{x}{\xi^2 + x^2},\ v_z = -\dot{w}(t)\frac{h}{\tan\theta}\frac{\xi}{\xi^2 + x^2} \tag{7}$$

where $\dot{w}(t)$ is the moving velocity of the projectile tip. The divergence of deviatoric stress is

$$div\mathbf{s} = \nabla\left[-\tau_s\ln\left(\frac{\xi^2 + x^2}{h^2}\right)\right] \tag{8}$$

where τ_s is the shear yield stress. The pressures in the elastic and plastic regions of target and the stress components are respectively determined as follows

$$\begin{aligned} p^p &= f(t) + \Omega(\zeta, x, t) - \tau_s\ln\left(\frac{\xi^2 + x^2}{h^2}\right) \\ p^e &= g(t) + \Omega(\zeta, x, t) \\ \sigma_{nn} &= -p + \frac{\tau_s\Psi_1}{\Psi_0}, \sigma_{tt} = -p - \frac{\tau_s\Psi_1}{\Psi_0}, \sigma_{nt} = \frac{\tau_s\Psi_2}{\Psi_0} \end{aligned} \tag{9}$$

where

$$\begin{aligned} \Omega(\zeta, x, t) &= -\frac{\rho h\dot{w}^2}{2\tan^2\theta}\frac{h + 2\xi\tan\theta}{\xi^2 + x^2} - \frac{\rho h\ddot{w}}{2\tan\theta}\ln\frac{h^2}{\xi^2 + x^2} \\ \Psi_0 &= \left(\bar{X} - 1\right)^2 + \tan^2\theta\bar{X}^2 \\ \Psi_1 &= \left(1 + \tan^2\theta\right)\bar{X}^2 - 2\bar{X} + \frac{1 - \tan^2\theta}{1 + \tan^2\theta} \\ \Psi_2 &= \tan\theta\cos 2\theta\bar{X}^2 - \tan\theta\left(2 + \cos 2\theta\right)\bar{X} + \sin 2\theta \end{aligned} \tag{10}$$

in (9), the functions of time $f(t)$ and $g(t)$ are determined by boundary conditions and in (10), $\bar{X} = X/h$ an $\bar{Y} = Y/h$ are the normalized coordinates.

The moving equation of projectile in z direction is given by

$$[M + A(w, \dot{w})]\ddot{w} = F(w, \dot{w}) \tag{11}$$

where $M = 2\rho_P hb(2L - h/\tan\theta)$ and ρ_P are the projectile mass and density. $F(w, \dot{w})$ is the resultant force subjected by projectiles in the positive z axial direction. According to the method of Yarin et al. (9), the motion of chisel-shape projectile with angle 2θ penetrating into the metallic target plate with thickness H can be solved. Thus, we obtain the resultant force $F(w, \dot{w})$ is

$$F(w, \dot{w}) = \begin{cases} 2bh\tau_s C_1(\eta_1) & (\zeta_0 \le w \le 0) \\ 2bh\tau_s C_2(\eta_2) & (-H \le w < \zeta_0) \\ 0 & (w < -H). \end{cases} \tag{12}$$

Furthermore, we may determine the relationships of the residual velocity and penetration depth varying with the initial impacting velocity as follows

$$U_r = \frac{1}{C_0}\left[C_0U_0^2 + C_3(\eta_2)\right]^{1/2} \quad (w \le -H)\cdot \tag{13}$$

and

$$P = \frac{hC_0^2U_0^2}{\eta_0\left[1 + 2\ln\left(2\mu/\tau_s\right)\right]}\cdot \tag{14}$$

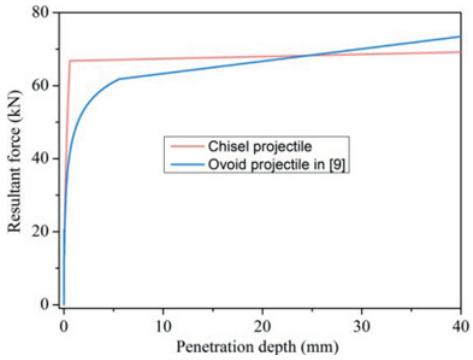

Figure 2. The variation of the resultant forces of the projectiles with different nose shapes with the penetration depth. The target thickness is 40 mm.

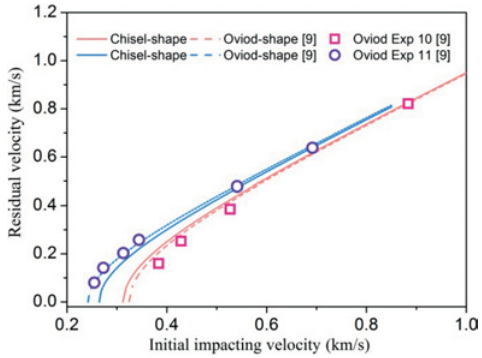

Figure 3. The effects of projectiles with different nose shapes on the residual velocities.

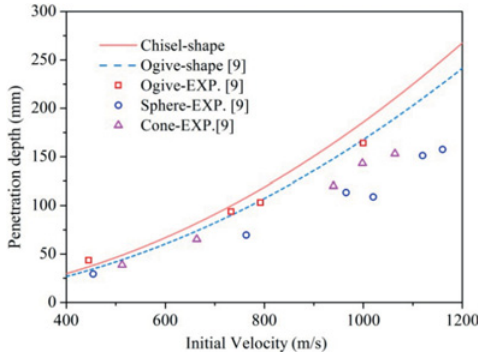

Figure 4. The relationships between the penetration depth and the initial impacting velocity.

In (12) to (14),

$$C_0 = \left(\frac{M + A}{4bh^2\tau_s}\eta_0\right)^{1/2},$$

$$C_1(\eta_1) = 1 + \ln\left[\eta_0^2\left(\frac{2\eta_1^2}{1 + \eta_1 - 2\eta_1^2}\right)^{2/3}\right]$$

$$C_2(\eta_2) = 1 + \ln\left[\eta_0^2\left(\frac{2\eta_2^2}{\tan\theta\,(\eta_2 + 1) + 2\eta_2^2}\right)^{2/3}\right]$$

$$C_3(\eta_2) = 1 - \frac{\eta_0}{h}\left[2\eta_2 \ln\eta_0 - (H + \zeta_0)\,C_2(\eta_2)\right]$$

$$\zeta_0 = -\frac{h\eta_2^2}{\eta_0 \tan\theta\,(\eta_2 + 1)},\ \eta_0 = \frac{\tau_s}{2\mu}$$

$$\eta_1 = \eta_0\left(1 - \frac{\zeta_0 - w}{h}\tan\theta\right),\ \eta_2 = \eta_0\left(1 + \frac{H}{h}\tan\theta\right) \quad (15)$$

where ζ_0 denotes the boundary between the elastic and plastic regions in target ahead the projectile nose.

3. Results and discussion

Figure 2 illustrates the variation of the resultant forces respectively caused by the chisel- and ovoid-shape projectiles with the penetration depth as striking the target of 40 mm thickness. The lengths of the projectile noses and bodies are respectively 5 mm and 25 mm. Since the contact area between the chisel nose and target is sufficient large, the force amplitude of the chisel-shape projectile reaches its peak value as the penetration depth is only 2 mm, and then it remains constant. The force of ovoid-shape projectile non-linearly increases in amplitude in initial penetration distance of the nose length 5 mm. Then, as the ovoid nose completely gets into the target which is denoted by the inflexion on the cover, the force increases linearly with the penetration depth. When the whole body of projectile gets into the target, the force amplitude exceeds that of the chisel-shape projectile, which implies that the chisel-shape projectile is favorable to the penetration of the target plate with large thickness comparing to the ovoid-shape projectile.

Figure 3 shows the effect of the chisel- and ovoid-shape projectiles on the residual velocity. For the comparison, these projectiles are assumed to have same masses but different lengths, and the target thickness is taken as 25.4 mm. Clearly, in the penetration process at high impacting velocities, the influence of projectile nose shapes on the residual velocities is not evident. However, at lower impacting velocities, the residual velocities of the chisel-shape projectile with larger length (blue line) are lower evidently then that of the ovoid-shape projectile. This is because that the work done by the drag force caused by target acting on the projectile is larger, whereas for the shorter ovoid-shape projectile in length (red line), the work done by drag force is less so that the influence is slight.

Figure 4 compares the theoretical result in this study and the studying results in [9] for the penetration mechanisms of different nose shape projectiles into semi-infinite target plates. It predicts that the chisel-shape projectile may have better penetration efficiency than that with other nose shapes at high impacting velocities. Particularly, the chisel-shape projectile has evident increasing tendency for the material dynamic failure of target plates with large thickness in the penetration process at high impacting velocity.

4. Numerical simulation

In order to further study the energy dissipation mechanisms of different projectiles striking a metallic target plates, numerical simulations were performed using the LS-DYNA finite element code [1]. Figure 5 shows the

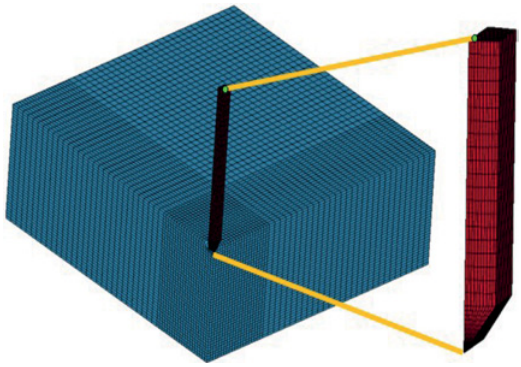

Figure 5. The finite element model of the chisel-shape projectiles penetrating into the target plate.

finite element model used in this simulation. Consider the symmetric property of the problem; a quarter part of the model is calculated for conserving computational time. Similarly, the projectiles with different nose shapes are assumed as rigid body and the nose shapes of projectiles simulated are chosen as spherical, conical and chisel-shapes. The mass of the projectile is about 63 g, diameter is 7.2 mm and the length is 48 mm. The target material is the 4340 steel and two kinds of target plate sizes are $240 \times 240 \times 6\,\text{mm}^3$ and $240 \times 240 \times 40\,\text{mm}^3$ respectively. The mesh comprises 8-node brick elements with reduced integration and stiffness-based hourglass control with exact volume integration. In the simulation for penetrating 6 mm target plate, the smallest element in the impact region has the initial size of $1 \times 1 \times 0.6\,\text{mm}^3$ and a total of 10 layer elements are distributed over the target thickness. In the case of the 40 mm target plate, the element size is $1 \times 1 \times 1\,\text{mm}^3$ and 40 layer elements are distributed in thickness.

Figure 6 shows the variation of the normalized kinetic energy with time in the penetration process of the target plate in 6 mm thickness. The kinetic energy of chisel- and spherical-shape projects decreases quickly when the penetration depth is less than the thickness of target plate and it begins to decrease for the conical-shape projectile when the penetration depth is near the thickness of target plate. For the chisel-and spherical-shape projectiles, when the penetrable lengths equal to 18.6 mm and 27.4 mm, the dissipation of the kinetic energy finish and, for the conical-shape projectile it is stopped as the penetrable length is larger than 38.2 mm. Thus, we can say that the chisel-shape projectile remains larger residual velocity, which means that it is in favor of the penetration of thick target plate. The simulation results in Fig. 7 shows that the sphere- and chisel-shape projectiles with the chisel angles 30°, 45° and 60° can penetrate through the target plate of 40 mm thickness but the penetration depth of the cone-shape projectile is 35 mm. The normalized kinetic energies of all kinds of projectiles decrease linearly with the penetration distance. The dissipations of kinetic energy for the sphere-shape and the chisel-shape 30° projectiles are almost identical. The loss of kinetic energy of chisel-shape projectile increases with the chisel angle increasing. The cone-shape projectile dissipates the less kinetic energy at the beginning stage of the penetration, however, most of

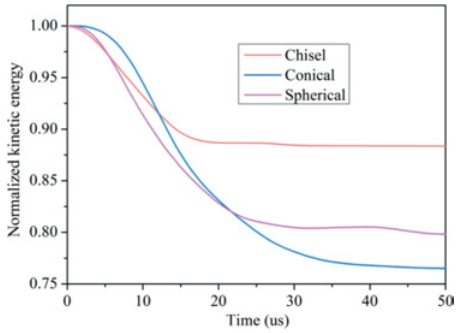

Figure 6. The variation of the normalized kinetic energy with time in the penetration process of the target plate in 6 mm thickness.

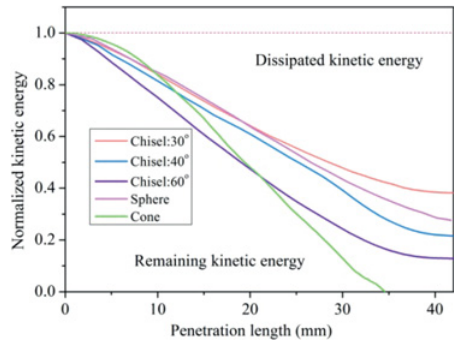

Figure 7. The variation of the normalized kinetic energy with the depth of penetration in the penetration process of the target plate in 40 mm thickness. The chisel angles are respectively 30°, 45° and 60°.

kinetic energy quickly dissipates in the later penetrating stage so that it cannot penetrate the target plate of 40 mm thickness. Therefore, the chisel-shape projectile has the ability for the penetration of thicker target plates and the cone-shape projectile is favorable to the penetration of thin target plate.

5. Conclusions

Through the analysis and numerical simulation study of the chisel-shape projectile penetrating a target plates with finite thickness, we have shown that, comparing to different nose shape projectiles, the chisel-shape projectile is favorable to penetrate the thick target plates at high impacting velocities; contrarily, the cone-shape projectile is to that of thin target plates at low impacting velocities. The simulation result shows that the sphere-shape and the chisel-shape 30° projectiles are almost identical of the energy dissipation behaviors in the penetration process of thick target plates.

References

[1] R.F. Bishop, R. Hill, N.F. Mott, J. Proceedings of the Physical Society, **57**(3): 147 (1945)
[2] J.N. Goodier, M. Stanford Research Institute (1964)
[3] M.J. Forrestal, D.Y. Tzou, J. International Journal of Solids and Structures, **34**,(31): 4127–4146 (1997)
[4] M.J. Forrestal, K. Okajima, V.K. Luk, J. Journal of applied mechanics, **55**: 755 (1988)

[5] Xiaowei, Chen, Guanjun, Liang, Yong Yao, et al, J. Chinese journal of theoretical and applied mechanics, **41**(1): 84-90 (2009)
[6] V.P. Alekseevskii, J. Explosion, and Shock Waves. 15 July 63 (1965)
[7] A. Tate, J. Me &. Phys. Solids, **17**, pp. 141 to 150 (1969)
[8] A. Tate, J. Me &. Phys. Solids, **15**, pp. 387 to 399 (1967)
[9] M. Ravid, S.R. Bodner, I. Holcman, J. International journal of engineering science, **25**(3): 473–482 (1987)
[10] M. Ravid, S.R. Bodner, I. Holcman, J. International journal of impact engineering, **15**(4): 587–603 (1994)
[11] A.L. Yarin, M.B. Rubin, Roisman I.V., J. International journal of impact engineering, **16**(4): 801–831 (1995)
[12] G. Yossifon, M.B. Rubin, A.L. Yarin, J. International journal of impact engineering, **25**(3): 265–290 (2001)
[13] M.B. Rubin, J. International Journal of Impact Engineering, **40**: 1–9 (2012)
[14] J.B. Jordan, C.J. Naito. J. International Journal of Impact Engineering, **63**: 63–71 (2014)